Three-dimensional stress state above and below the plate boundary fault after the 2011 Mw 9.0 Tohoku earthquake

AUTHOR(S):

Lin, Weiren; Yamamoto, Yuhji; Hirose, Takehiro

CITATION:

Lin, Weiren ...[et al]. Three-dimensional stress state above and below the plate boundary fault after the 2011 Mw 9.0 Tohoku earthquake. Earth and Planetary Science Letters 2023, 601: 117888.

ISSUE DATE:

2023-01-01

URL:

http://hdl.handle.net/2433/277281

Earth and Planetary Science Letters 601 (2023) 117888

Contents lists available at ScienceDirect

Earth and Planetary Science Letters

www.elsevier.com/locate/epsl

Three-dimensional stress state above and below the plate boundary fault after the 2011 Mw 9.0 Tohoku earthquake

Weiren Lin [a,*], Yuhji Yamamoto [b], Takehiro Hirose [c]

[a] Graduate School of Engineering, Kyoto University, Kyoto 615-8540, Japan
[b] Center for Advanced Marine Core Research, Kochi University, Nankoku, Kochi, Japan
[c] Kochi Institute for Core Sample Research (X-star), Japan Agency for Marine-Earth Science and Technology (JAMSTEC), Nankoku, Kochi, Japan

ARTICLE INFO

Article history:
Received 20 June 2022
Received in revised form 7 October 2022
Accepted 24 October 2022
Available online xxxx
Editor: R. Bendick

Keywords:
Tohoku earthquake
three-dimensional stress state
above and below plate boundary fault
anelastic strain recovery
JFAST
IODP

ABSTRACT

The Integrated Ocean Drilling Program conducted Expedition 343 and 343T, named the Japan Trench Fast Drilling Project (JFAST), to drill through the plate boundary fault that ruptured during the 2011 Mw 9.0 Tohoku earthquake in the area with the largest fault slip displacement near the Japan trench. Analyses of breakouts observed from borehole C0019B produced postearthquake stress states above the plate boundary fault between the subducting Pacific plate and overriding North American plate. To supplement the lack of stress data below the rupture zone of the earthquake, we conducted core-based three-dimensional stress measurements by the anelastic strain recovery (ASR) method using four whole-round core samples of sediments, of which three samples were located above, but one sample was located below the plate boundary fault in borehole C0019E. As a result of the stress measurements, the postearthquake three-dimensional stress magnitudes at ~802 and ~828 meters below seafloor (mbsf) across the plate boundary fault at ~820 mbsf reveal a normal faulting stress regime. The differences between the three-dimensional intermediate principal stress and the minimum principal stress at the two depths are less than 1 MPa, suggesting a complete release of horizontal tectonic stresses that accumulated before the earthquake. In addition, the maximum horizontal stress S_{Hmax} azimuth N115°E at ~828 mbsf below the plate boundary fault from ASR measurements shows consistency with the S_{Hmax} azimuth N139 ± 23°E (mean ± standard deviation) at ~550–810 mbsf from breakout analyses above the fault. Taken together with the similar stress magnitudes at ~802 and ~828 mbsf, we interpret that the postearthquake stress states are almost the same in the sediments above and below the plate boundary fault. In other words, the stress state in terms of both orientation and magnitude is continuous across the fault. At a shallower depth of ~177 mbsf in the slope sediments, the ASR stress data reveal a "stress state at rest", which is likely free from tectonic effects of plate subduction, suggesting that the stress state was reset by the great coseismic displacement of ~50 m slipped during the Tohoku earthquake.

1. Introduction

During the 11 March 2011 Mw 9.0 Tohoku-Oki, Japan, earthquake, the plate boundary megathrust ruptured and reached the sea floor at the axis of the Japan trench (Kodaira et al., 2012). The earthquake produced a maximum coseismic slip of >50 m close to the Japan trench, triggering a devastating tsunami (Fujiwara et al., 2011; Lay et al., 2011; Iinuma et al., 2012). Before the 2011 Tohoku earthquake, it was commonly known that each earthquake generally released only part of the stress driving the seismogenic fault (Brodsky et al., 2017). However, this exceptionally large rupture appears to have released all of the accumulated stress from the subduction of the Pacific plate beneath the North American plate (Hasegawa et al., 2011, 2012; Brodsky et al., 2017).

To understand the mechanisms more clearly for the record-breaking displacement of the coseismic slip, the Integrated Ocean Drilling Program (IODP, known as the International Ocean Discovery Program from 2013) conducted Expedition 343 and 343T, named the Japan Trench Fast Drilling Project (JFAST), to drill through the plate boundary fault that ruptured during the Tohoku earthquake mainshock (Mori et al., 2012). This drilling from the seafloor under an ~7 km water depth was rapidly undertaken by the drilling vessel (D/V) *Chikyu* approximately one year after the earthquake at site C0019 (Chester et al., 2012). The project investigated the mechanisms of the great coseismic slip that caused

* Corresponding author at: Graduate School of Engineering, Kyoto University, C1-1-109 Kyoto Daigaku Katsura, Nishikyo-ku, Kyoto, Kyoto 615-8540, Japan.
E-mail address: lin@kumst.kyoto-u.ac.jp (W. Lin).

https://doi.org/10.1016/j.epsl.2022.117888
0012-821X/

the devastating tsunami by conducting stress measurements in the borehole, sampling the plate boundary fault, and making temperature measurements across the ruptured fault (Mori et al., 2014).

Generally, tectonic stress slowly builds up along a seismogenic fault until it reaches the fault strength, and then an earthquake occurs by a sudden release of stress at the fault plane and in rock formations around the fault (e.g., Kanamori and Brodsky, 2001). The amount of coseismic stress release directly determines the release of elastic energy stored in rock formations around the fault and governs coseismic displacement along the fault. Knowledge of the stress state before, during and after a major earthquake enhances our understanding of the mechanisms of earthquake occurrence and rupture propagation (e.g., Brodsky et al., 2020). In the JFAST project conducted after the 2011 earthquake, the postearthquake stress states based on borehole breakout analyses have been obtained (Lin et al., 2013; Brodsky et al., 2017). Breakouts are borehole wall compressive failures 'naturally' induced by drilling under real in situ conditions and thus are good stress indicators if available. Absence of a breakout, however, cannot create stress state data. Unfortunately, breakouts clear enough for analysis did not form below the plate boundary fault in the JFAST borehole, and therefore, the stress state could not be determined in the depth range below the fault (Lin et al., 2013; Brodsky et al., 2017).

An applicable core-based three-dimensional method to measure stress acting on a drill core is the anelastic strain recovery (ASR) method. We considered this method to be able to supplement the lack of stress data below the fault. The principle behind the ASR method is that time-independent elastic strain is released first instantaneously, followed by a more gradual or time-dependent recovering of anelastic strain, also called "relaxation", after a rock core is drilled out (e.g., Matsuki, 2008; Gao et al., 2014). The ASR stress measurement takes advantages of the time-dependent strain and of a three-dimensional method, and has been successfully applied in several IODP expeditions (e.g., Byrne et al., 2009; Yamamoto et al., 2013; Oohashi et al., 2017) and other drilling projects (e.g., Matsuki and Takeuchi, 1993; Lin et al., 2006, 2007; Cui et al., 2014; Nagano et al., 2015; Sun et al., 2017; Zhang et al., 2022). Here, to determine three-dimensional stress states both above and below the plate boundary fault after the Tohoku earthquake, we collected four whole-round core samples from site C0019 of JFAST and conducted stress measurements by the ASR method onboard D/V *Chikyu*. Because the ASR method measures the anelastic strain caused by the stress release, it determines the stress state at the time of drilling, namely, the postearthquake stress in this study.

2. Methods

2.1. Tectonic background

In the Japan trench subduction zone, the Pacific plate is subducting west-northwestward beneath the North American plate at a high rate of ~9 cm/yr (e.g., Loveless and Meade, 2010; Argus et al., 2011). The relatively higher subduction rate induces a wider cold plate interface extended to great depths, thus resulting in a wider area of the frictionally coupled portion in the seismogenic subduction zone (e.g., Wang and Suyehiro, 1999). Before the 2011 Mw 9.0 Tohoku earthquake, M7-class earthquakes typically repeated there in approximately 30-year intervals (Yamanaka and Kikuchi, 2004).

As a result of the convergence direction of the Pacific and North American plates, contraction in margin normal direction is widely observed in northeast Japan by geodetic measurements (e.g., Yoshida et al., 2015). This suggests a margin normal (i.e., parallel to the direction of the plate convergences) compressional stress environment in the Japan trench subduction zone. In subduction zones, especially in offshore areas, the stress state is mainly evaluated by focal mechanisms and/or geodetic data analyses (e.g., Townend and Zoback, 2006; Terakawa and Matsu'ura, 2010; Hasegawa et al., 2011, 2012; Yoshida et al., 2012). Except for previous studies conducted in the JFAST project (Lin et al., 2013; Brodsky et al., 2017), stress-related reports from borehole drilling are limited in the offshore area (e.g., Lin et al., 2011).

2.2. JFAST (IODP Expedition 343) and core samples

The drilling site C0019 of JFAST (IODP Expedition 343) is located in an area of the largest coseismic slip zone of more than 50 m, ~93 km seaward of the epicenter of the Mw 9.0 Tohoku earthquake mainshock and ~6 km landward of the Japan trench axis (Fig. 1). Site C0019 is located directly above a horst block, approximately 1.2 km west of a normal fault boundary between the horst and adjacent graben centered under the trench (Fig. 2). The water depth at site C0019 is 6889.5 m (Expedition 343/343T Scientists, 2013b). At this location, three boreholes C0019B, D and E drilled within a narrow area of <30 m on the seafloor successfully penetrated the plate boundary fault between the subducting Pacific plate and the overriding North American plate. The three boreholes thus enabled geophysical logging (Logging While Drilling, LWD), long-term temperature monitoring and core sampling (Expedition 343/343T Scientists, 2013a; Lin et al., 2013; Fulton et al., 2013; Chester et al., 2013; Ujiie et al., 2013).

The borehole C0019E dedicated to coring retrieved a total of 21 cores, resulting in a total of 51 m long cores from both the hanging wall and the footwall of the plate boundary fault (Fig. 3). An approximately one-meter-long section of the scaly clay unit was recovered in core 17R (343_C0019E-17R-1) from depths of 821.50 to 822.65 meters below seafloor (mbsf) and was interpreted as the subduction plate boundary fault ruptured during the Tohoku earthquake mainshock (Chester et al., 2013). The intensely sheared fault itself was not completely recovered but has a maximum thickness of <4.86 m, and the top of the plate boundary fault was identified at ~820 mbsf in C0019E (Rowe et al., 2013 and Chester et al., 2013).

The four whole-round core samples used for ASR stress measurements (called ASR-1 – ASR-4) were collected from C0019E-1R1 (~177 mbsf), C0019E-5R1 (~697 mbsf), C0019E-13R1 (~802 mbsf) and C0019E-19R2 (~828 mbsf) (Fig. 3 and Table 1). The three core samples at shallower depths were retrieved from the hanging wall of the fault. The shallowest core, ASR-1, was from the slope sediments, whereas ASR-2 and ASR-3 were from the wedge sediments (the frontal prism) of the overriding North American plate. In contrast, the deepest core sample ASR-4 was from the underthrust sediments, a few meters below the plate boundary fault. All four core samples (see their photos shown in Fig. S1 in the supplemental material of this paper) are mudstone with relatively high porosities from ~45 to ~67% and lower wet bulk densities of 1.52–1.92 g/cm^3 (Table 1). All the ASR samples are visually homogeneous and isotropic. The same four core samples after ASR measurements in this study were reused for thermal property measurements; the results revealed that very slight differences were recognized between the thermal conductivities in the axial and radial directions of the core samples measured in an anisotropic mode (Lin et al., 2014). Differences between thermal conductivities in the orthogonal directions of the four samples remained small, and the maximum difference was seen in ASR-2 among the four samples, to be ~4% of the mean thermal conductivity in the two directions. In addition, onboard P-wave velocities (V_p) measured in vertical and horizontal directions of cubic samples from the same core No. 5R, 13R and 19R as ASR-2, 3 and 4, respectively showed that relative difference of V_p in the two di-

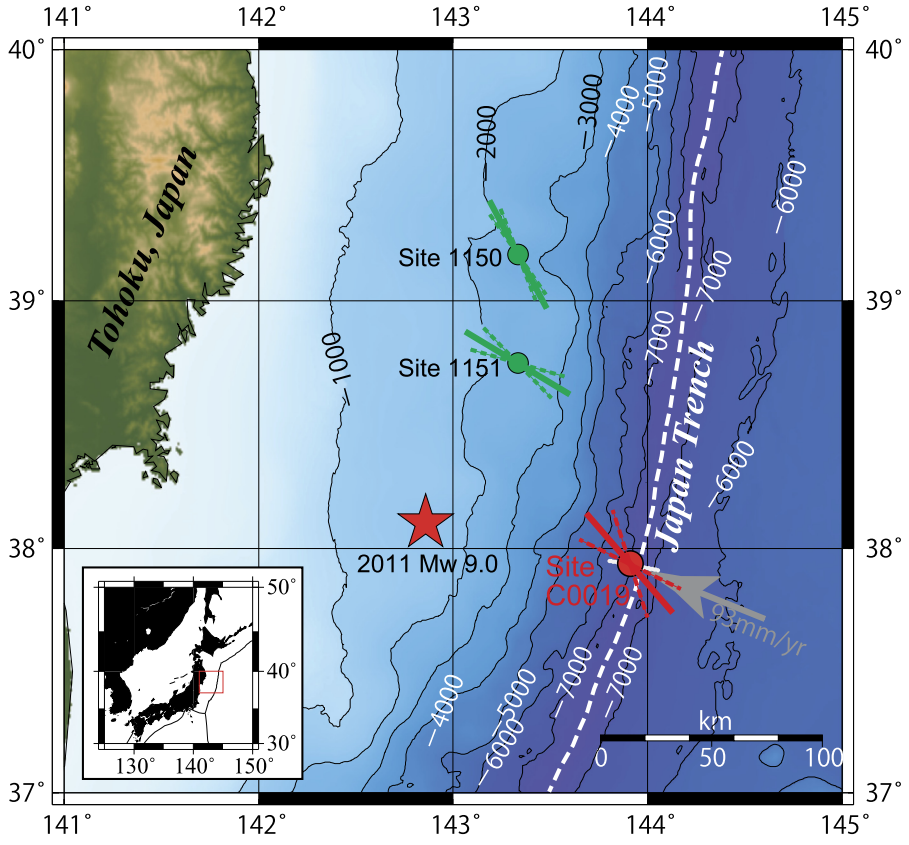

Fig. 1. Location of drilling site C0019 of JFAST and S_{Hmax} orientation above the plate boundary fault. Red solid and dashed lines show the mean S_{Hmax} orientation in Log unit IIb and one standard deviation (SD), respectively (after Lin et al., 2013). Green circles and lines indicate ODP sites drilled in 1999 and their S_{Hmax} orientations prior to the 2011 Tohoku earthquake (after Lin et al., 2011). Red star shows the epicenter of the 2011 earthquake mainshock, the gray arrow shows relative plate motion (Argus et al., 2011). The white line around site C0019 indicates the location of Fig. 2. This map was modified from Lin et al., 2013 and Lin et al., 2014. (For interpretation of the colors in the figure(s), the reader is referred to the web version of this article.)

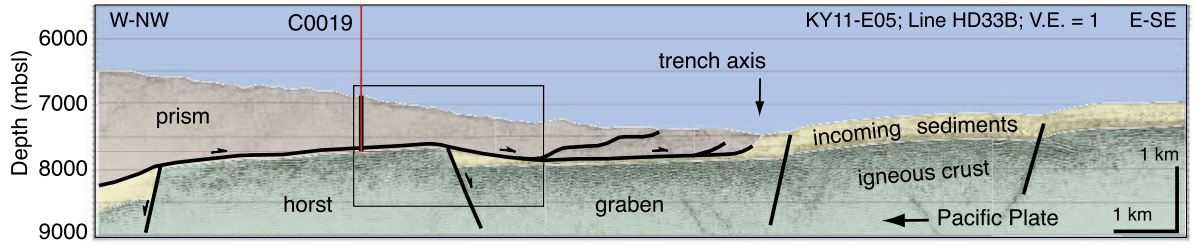

Fig. 2. Interpreted inline seismic profile (HD33B) crossing site C0019 (after Chester et al., 2013). It shows the location of the boreholes (red vertical lines), frontal prism and trench, the normal-faulted basal pelagic sediments and oceanic basalt, and the interpreted location of the plate boundary fault and associated faults in the sediments. mbsl: meters below sea level; V.E.: vertical exaggeration. Subducting Pacific plate dips gently ~5°; landward lower trench slope dips ~7° (Lin et al., 2013).

rections defined as "$(V_{p\text{-vertical}} - V_{p\text{-horizontal}})/V_{p\text{-mean}}$" were ~5% for 5R and 1–2% for 13R and 19R (Expedition 343/343T Scientists, 2013b). Therefore, we consider that the ASR samples used in this study are almost isotropic.

2.3. ASR measurements

To measure recovery of the anelastic strain caused by stress release accompanying drilling of the core samples in at least six independent directions, we glued strain gauges on the core cylindrical surface in the same layout shown in Fig. S2 as our previous studies (e.g., Lin et al., 2007; Byrne et al., 2009; Yamamoto et al., 2013; Nagano et al., 2015; Sun et al., 2017). Because the anelastic stain recovery rate decreases with time after in situ stress release, we must conduct ASR measurements as soon as possible after core samples are retrieved. Therefore, we performed the measurements onboard D/V *Chikyu*. After minimum core handling procedures, including X-ray CT scanning and MSCL (multisensor core logger) measurement, we immediately began sample preparations for the ASR measurements using the cores. As a result, we started ASR measurements three–five hours after the core sample was "on deck" mainly depending on their core handling time, corresponding to six–eight hours from the in-situ stress release. The ASR measurements were conducted continuously for approximately three weeks for ASR-1, which was retrieved earlier, and approximately two weeks for the others. The same ASR measurement system as our previous IODP studies (e.g., Byrne et al., 2009; Yamamoto et al., 2013; Oohashi et al., 2017) was used, with a total of 120 strain measurement channels to enable ASR measurements for six core samples simultaneously (Figs. S3 and S4).

To observe the strain recovery caused by stress release, it is important to exclude deformation (strain) caused by temperature change for long-term (approximately three or two weeks) measurements. Thus, we set the ASR core samples in a constant tem-

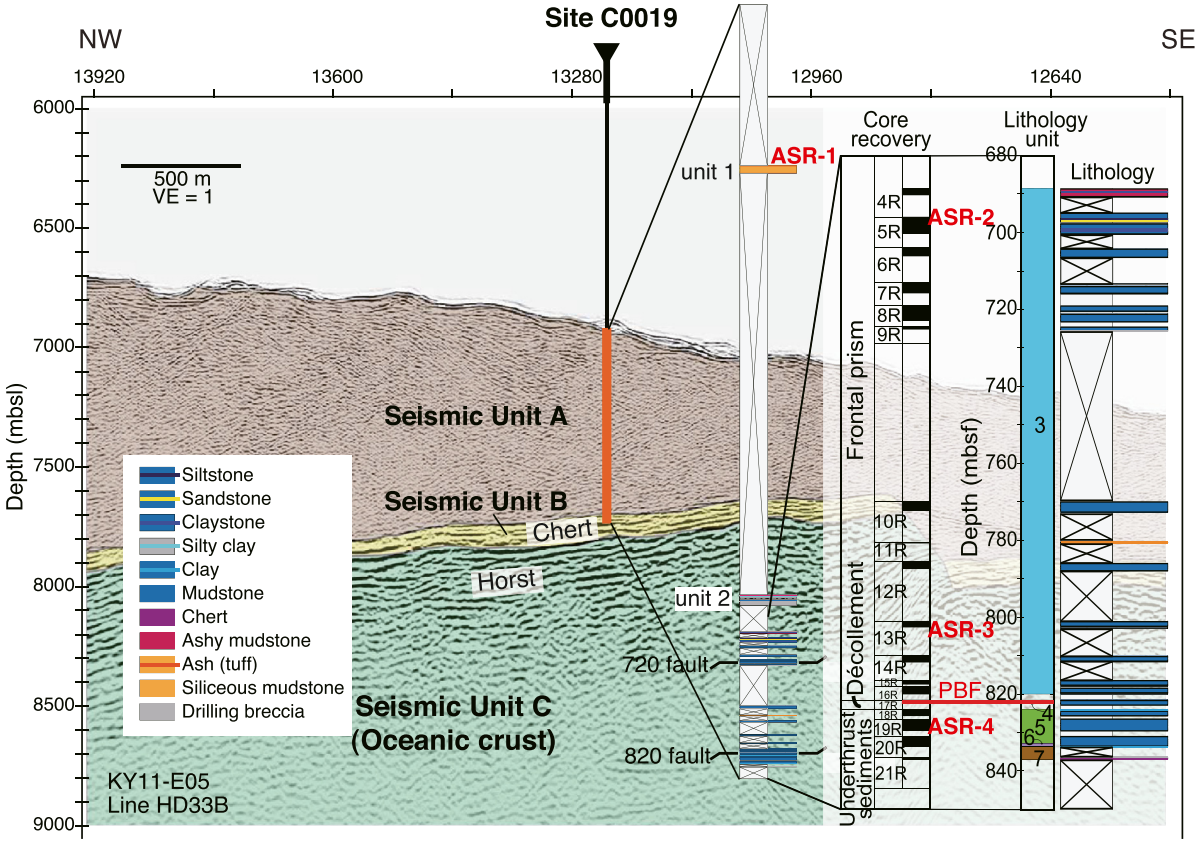

Fig. 3. Borehole C0019E and locations of core samples ASR-1–4 used in this study. Graphical representation of hole penetration, with intervals of the borehole cored on seismic section Line HD33B (modified from Expedition 343/343T 2013a, Yang et al., 2013 and Lin et al., 2014). Inset indicates coring run numbers from 4R to 21R; black bar in a coring depth range shows the total length of the recovered cores and the white part denotes the length of the core not recovered. Lithology determined on the basis of visual core description is represented in color within the lithologic column. Thick red line and 'PBF' show the depth of the plate boundary fault. Seismic units A (the frontal prism), B (chert below the decollement), and C (oceanic crust) are shown with brown, yellow, and green shading, respectively. VE and mbsl are the same as those in Fig. 2.

Table 1
Sample ID, Core ID, depth, lithology, basic physical properties and core reorientation results by using rock remanent magnetization of the four ASR core samples.

Sample ID	Core ID[a]	Depth (mbsf)	Lithology[b]	Physical properties			Core reorientation by using remanent magnetization					
				Wet bulk density (g/cm^3)	Grain density (g/cm^3)	Porosity (%)	Number of Sub-samples[c]	Declination (°)	Inclination (°)	α_{95}	Polarity	Orientation of ASR line
ASR-1	C0019E-1R-1, 18–34 cm	~177	olivegray siliceous mudstone	1.52	2.60	67.3	8	248.5	43.7	3.0	Normal	N111.5°E
ASR-2	C0019E-5R-1, 102–117 cm	~697	gray mudstone	1.89	2.63	45.2	6	354.1	56.6	2.8	Normal	N5.9°E
ASR-3	C0019E-13R-1, 50–60 cm	~802	gray mudstone	1.92	2.66	44.7	5 5	230.5 242.4	−16.0 −10.4	4.3 7.0	Reversed Reversed	– –
ASR-4	C0019E-19R-2, 73–86 cm	~828	brown mudstone	1.86	2.54	45.4	7	67.1	49.6	2.4	Normal	N292.9°E

[a] Core ID denotes borehole, core and section numbers, top and bottom depths of the core sample in the section.
[b] Lithologies of the core samples are after Expedition 343/343T Scientists (2013b).
[c] Subsamples were formed as ~2.5 cm cube, divided from a 2.5 cm thick core disk cut from the ASR samples. Usually, eight cubic subsamples were used for each remanent magnetization measurement. Number of Subsamples here denotes the numbers of successful measurement.

perature chamber filled with water that was circulated between a circulator and the chamber (a water bath) and cooled/heated to keep the temperature constant in the circulator (Figs. S3 and S4). Fig. S5 shows the results of temperature change during the ASR measurement duration. Although room temperature in the laboratory in D/V *Chikyu* changed in a wide range of ~21–27 °C, the temperature in the water bath where the ASR samples were installed varied in a very narrow range of 23.7–23.9 °C. In addition, to monitor the strain measurement system state, we also measured strain variation using a dummy sample that did not have anelastic strain occurring by stress release. The measured strain data did not have a distinct change with time, suggesting that no drift in our strain measurement system occurred during the duration (Fig. S6).

2.4. Core reorientation

To restore stress orientations determined from ASR core samples to the geographic coordinate system, we carried out paleomagnetic measurements in a shore-based laboratory after the ASR measurements using the same procedure proposed by Sugimoto et al. (2020). Stepwise alternating field demagnetization of natural remanent magnetization revealed that three core samples ASR-1,

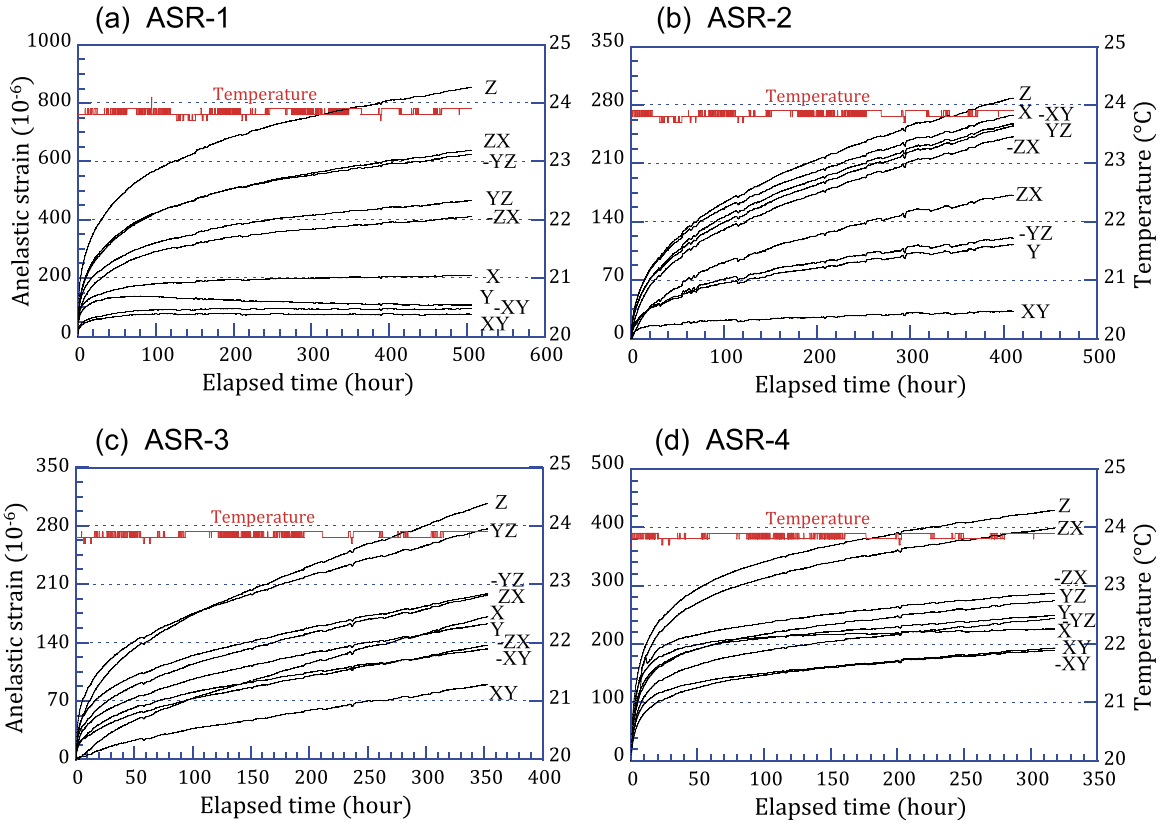

Fig. 4. Raw data of anelastic strain recovery with time elapsing of core samples ASR-1–4, respectively. Labels of capital letters beside the curves indicate measurement directions of anelastic strains shown in Fig. S2.

2 and 4 from ~177, ~697 and ~828 mbsf, respectively, record paleomagnetic inclinations that are in reasonable agreement with the inclination of 57.3° expected from the geocentric axial dipole field at the latitude of drilling site C0019 (37.9°N, Table 1 and Fig. S7 (a–c)). Sedimentary rocks are known to record paleomagnetic fields by averaging out secular variations in the geomagnetic field. Thus, the paleomagnetic direction of the rocks corresponds to the direction of the magnetic field generated by the geocentric axial dipole, the declination of which is equal to zero everywhere on the globe. Thus, it is considered that declinations determined by paleomagnetic measurements can be used to restore core orientation for these three samples. In contrast, the palaeomagnetic inclination determined for core sample ASR-3 from ~802 mbsf was not consistent with the latitude of the sample recovery site. This suggests that the sediments have rotated since deposition; therefore, the directions of natural remanent magnetization in ASR-3 reflect the orientation before its rotation (e.g., at the time of its deposition) rather than the current direction. Thus, the reorientation result is difficult to be used to restore core sample ASR-3. To confirm this result, we conducted the same paleomagnetic measurement again using the other disc-shaped subsample cut from the same core sample ASR-3, which showed a similar result (Table 1 and Fig. S7 (d and e)).

3. Results

3.1. Anelastic stain recovery (ASR)

The anelastic strains measured in nine directions shown in Fig. S2, including six independent directions, for all four core samples were extensional. All strain-time curves varied convexly upward and similarly with increasing time (Fig. 4). The magnitudes of the anelastic strains were dependent on the strain measurement directions and had a typical value of several hundred microstrains (10^{-6}) measured for approximately two weeks. Generally, the values of anelastic strains in the vertical direction for the four core samples (labeled "Z" in Fig. 4 (a–d)) were higher than those in the other directions (refer to Fig. S2). This observation implies that the stress component in the vertical direction may be large in comparison with those in the other directions. With regard to a comparison between the recovered anelastic strain values at the same elapsed time (e.g., approximately 350 hours), the strain in the Z direction as a representative strain of ASR-1 (~177 mbsf) reached approximately twice that of the other three samples because the mudstone from the much shallower formation was weakly compacted and had lower density and higher porosity (Table 1).

During the three weeks covering whole ASR measurement durations for the four samples, the temperature of core samples in the constant temperature chamber (the water bath) varied in a small range of ~0.2 °C. Nevertheless, the anelastic strain curves revealed some abrupt changes (e.g., ~390, ~300, ~240, ~200 hours for ASR-1, 2, 3, 4, respectively) caused by the temperature change (Fig. 4, especially (b) and (c)). This influence from the temperature change on each core sample was approximately the same and thus was recognized clearly for ASR-2 and ASR-3 at a smaller anelastic strain scale (350 microstrains at full scale in Fig. 4 (b) and (c) but not clear for ASR-1 at the larger scale (Fig. 4(a)). Although such minor influences by temperature change were recognizable locally, the overall trends of anelastic strain recovery were not influenced, and there is no need to conduct corrections, as Lin et al. (2006) did. Therefore, principal anelastic strains and the mean strain can be calculated for the four ASR core samples from the raw anelastic strain data (Fig. 5).

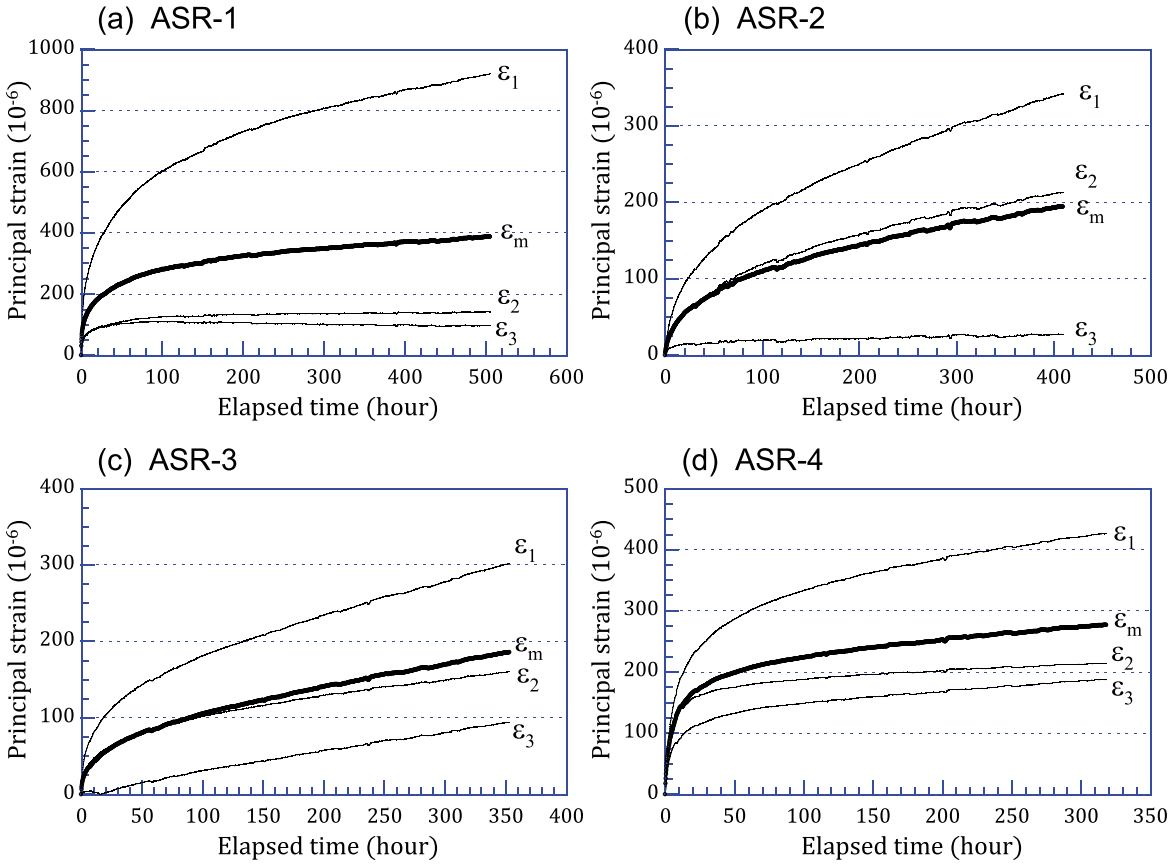

Fig. 5. Three-dimensional principal anelastic strains (ε_1, ε_2, ε_3) and the mean strain (ε_m) versus time elapse. These data were analyzed from the raw data shown in Fig. 4 for the four ASR core samples.

3.2. Stress orientations

For isotropic and liner viscoelastic materials, the principal stress orientations are the same as the principal anelastic strain orientations (Matsuki, 1991). Therefore, the three-dimensional principal stress orientations and two-dimensional stress azimuths in the horizontal plane were determined from the ASR measurements for the four core samples from four depths at site C0019 (Fig. 6 and Table S1). This stress dataset shows the stress state at the time of core stress release (the time of drilling of IODP Expedition 343; 14th – 22nd May 2012), i.e., the stress state after the 2011 Tohoku earthquake. The orientations of maximum stress σ_1 at the three depths of ASR-1, 3, 4 are approximately vertical, and their intermediate stress σ_2 and the minimum stress σ_3 are in the horizontal plane (Fig. 6 (a), (c) and (d)). The result of ASR-2 shows that σ_1 and σ_2 are oblique with a similar dip (plunge), but σ_3 is horizontal. Overall, at the C0019 site, the maximum principal stress is approximately in the vertical direction. The stress state after the earthquake is in a normal faulting stress regime. This stress state from ASR measurements is consistent with the results of borehole breakout originally analyzed by Lin et al. (2013) and reanalyzed by Brodsky et al. (2017).

Except for ASR-3, where the horizontal stress orientation cannot be restored to geographic coordinates, the maximum horizontal stress S_{Hmax} azimuths range from WNW-ESE to NNW-SSE. Generally, these S_{Hmax} azimuths show good consistency with the stress data obtained by Lin et al. (2013) (see the red lines in Fig. 1).

3.3. Stress magnitude

Based on two assumptions similar to our previous studies (Lin et al., 2007; Yamamoto et al., 2013), we estimated the three-dimensional principal stress magnitudes and the two horizontal principal stress magnitudes for the four depths where the ASR core samples were retrieved (Table 2). For the details of the calculation method, including equations, see the methodology chapter in Yamamoto et al. (2013). First, we assumed that the total stress magnitude S_v in vertical direction is equal to the total weight above the depth, including both rocks (sediments) and seawater, i.e., the integral of the density (in the case of rocks, water saturated bulk density) from the sea surface to depth. Second, the ratio of the two ASR compliances of volumetric and shear deformation modes was assumed to be a constant, i.e., $J_{av}(t)/J_{as}(t)$ = constant. Based on results of laboratory experiments under uniaxial compression, Matsuki (2008) found that the ratio of $J_{av}(t)$ and $J_{as}(t)$, regardless of the rock type, approaches an almost constant value that converges in a narrow range (0.64 ± 0.14) as time elapses. Therefore, we estimated the stress magnitudes based on $J_{av}(t)/J_{as}(t)$ = 0.50, 0.64 and 0.78 (see Table 2). Similar to the result of a simulation to examine the effect of the ratio variation of $J_{av}(t)/J_{as}(t)$ from 1/3 to 1 by Lin et al. (2006), the estimated stress magnitudes in this study did not change significantly.

Because the density log failed and only limited core samples were available at site C0019 of the JFAST drilling project, Expedition 343/343T Scientists (2013b) established depth profiles of porosity and density based on resistivity log data (Fig. S8). We estimated the S_v magnitudes for the four depths by this density depth profile and hydrostatic pore pressure p_0 based on an average sea water density of 1.040 g/cm^3 as in Lin et al. (2013) (see estimated p_0 and S_v values in Table 2).

To consider the stress magnitudes at the four depths, we plot the maximum and minimum horizontal stresses on stress polygons at each depth in Fig. 7. The fundamental concept of the stress

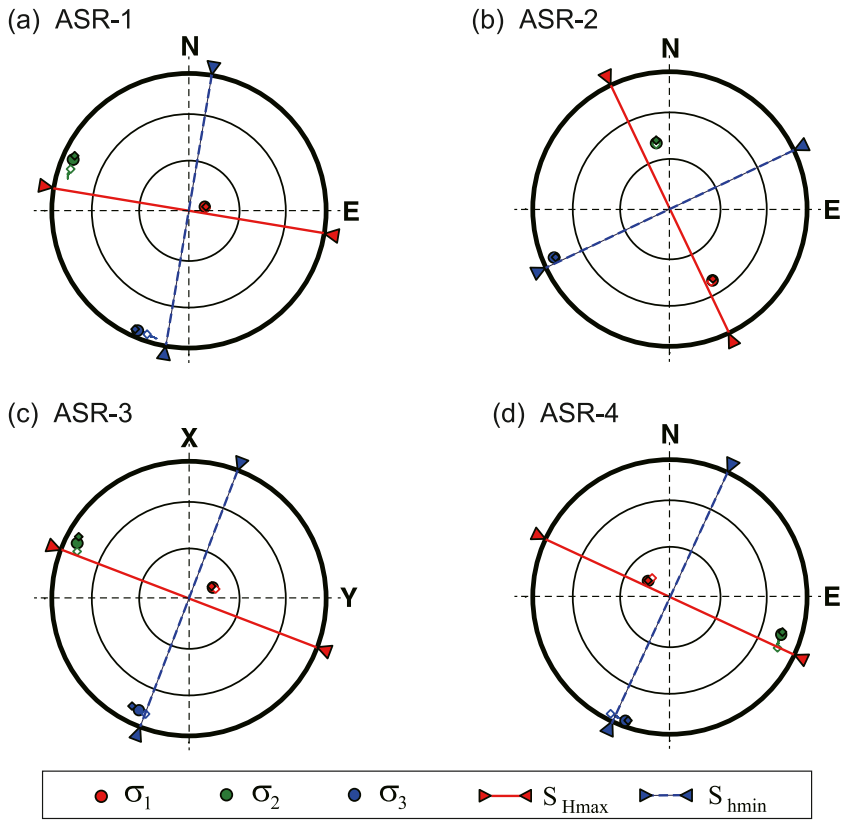

Fig. 6. Lower hemisphere, equal area projections of principal stress orientations determined by ASR measurements. Open and solid diamonds for each principal stress (σ_1, σ_2, σ_3) show the orientation at the start and end of the ASR measurement, respectively. Mean orientations of the principal stresses are shown by larger circles. The labels of "X" and "Y" in (c) denote local coordinate system of the core sample, meaning that core reorientation for ASR-3 failed.

Table 2
Stress magnitude measurement results of the four core samples by the ASR method. Stress magnitudes calculated vary slightly with assumed values of Jav(t)/Jas(t). The magnitudes shown in bold numbers for Jav(t)/Jas(t)=0.64 were used as their representatives.

Sample ID	Depth (mbsf)	p_0 (MPa)	S_V (MPa)	Jav(t)/ Jas(t)	σ_1 (MPa)	σ_2 (MPa)	σ_3 (MPa)	S_{Hmax} (MPa)	S_{hmin} (MPa)
ASR-1	~177	72.1	73.0	0.50	73.1	72.5	72.4	72.5	72.5
				0.64	**73.1**	**72.4**	**72.4**	**72.4**	**72.4**
				0.78	73.1	72.3	72.3	72.3	72.3
ASR-2	~697	77.4	82.1	0.50	83.0	81.6	79.7	82.4	79.8
				0.64	**83.2**	**81.5**	**79.1**	**82.5**	**79.2**
				0.78	83.4	81.4	78.6	82.6	78.7
ASR-3	~802	78.5	83.9	0.50	84.1	82.4	81.7	82.5	81.8
				0.64	**84.1**	**82.1**	**81.2**	**82.2**	**81.3**
				0.78	84.1	81.2	80.8	81.9	80.9
ASR-4	~828	78.7	84.4	0.50	84.6	82.8	82.6	82.9	82.6
				0.64	**84.6**	**82.5**	**82.2**	**82.6**	**82.2**
				0.78	84.6	82.1	81.8	82.3	81.8

polygon showing limits of the stress magnitude is that the possible stress magnitude acting on rocks cannot exceed the rock's failure criterion for which the Mohr–Coulomb criterion is usually applied (Zoback, 2007). Certainly, the size of the stress polygon is dependent on the rock internal frictional coefficient (see Fig. S9). Here, we take a value of 0.6 (the same as that used in Lin et al., 2013) for the rock internal frictional coefficient to draw the stress polygons shown in Fig. 7. As a result, the Andersonian stress state in which one principal stress axis is vertical stress at the four depths is located in the area of the normal faulting stress regime (ASR-1, 3 and 4) or very close to the area (ASR-2). Although vertical stress of ASR-2 was not one of the three principal stresses, we conveniently indicated its two horizontal principal stresses S_{Hmax} and S_{hmin} which are nearly equal to three-dimensional maximum and minimum principal stresses σ_1 and σ_3, respectively (see Table 2) on the stress polygon (Fig. 7(b)).

4. Discussion and implication of ASR stress data

4.1. Comparisons of stress orientations with previous breakout data

In the LWD borehole C0019B ~6 m away from the coring borehole C0019E, where core samples for ASR measurements were retrieved (Expedition 343/343T, 2013b), abundant breakouts (drilling-induced compressive failures) as stress indicators were observed from the borehole wall resistivity images (Lin et al., 2013; Brodsky et al., 2017). The cumulative length of all borehole breakouts reached approximately 96 m, corresponding to approximately

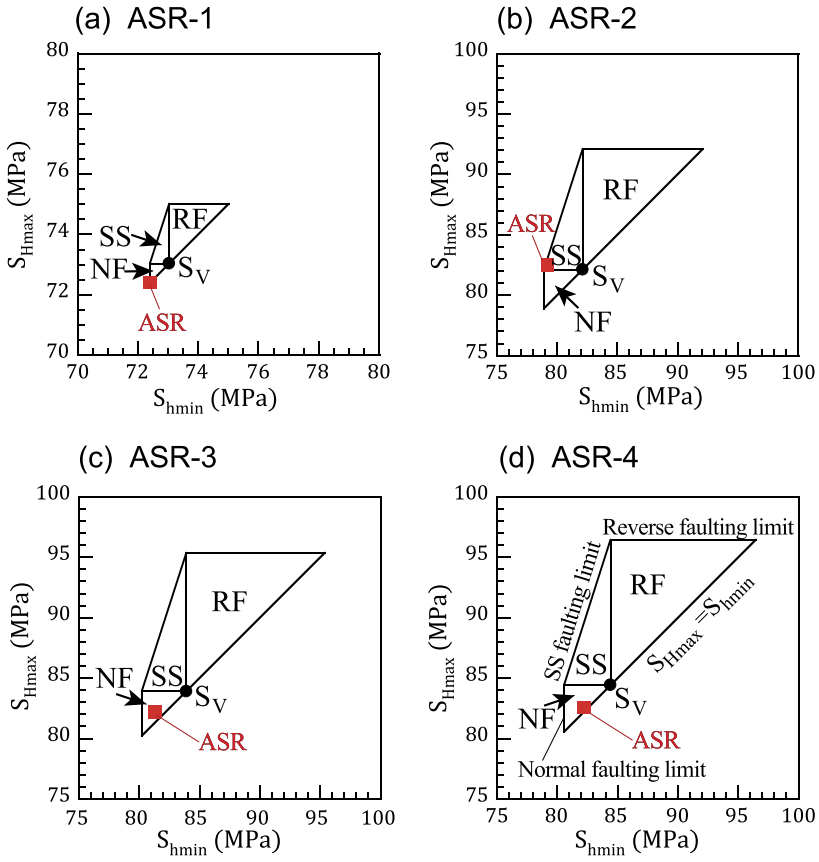

Fig. 7. The plot of S_{Hmax} and S_{hmin} magnitudes by ASR measurements in stress polygon domains. Stress polygons are based on the Anderson theory of faulting with coefficients of internal friction of 0.6 (Lin et al., 2013). As the stress state must lie inside the polygon defined by the vertical stresses (S_V) and assumed coefficients of internal friction, only a restricted area of values of S_{Hmax} and S_{hmin} is possible. Three triangle areas labeled as RF, SS and NF in the polygons show the reverse faulting (RF), strike-slip faulting (SS) and normal faulting (NF) stress regimes, respectively.

11% of the total borehole length (Lin et al., 2013). Breakouts were observed in the depth range of ~44–813 mbsf which is ~7 m above the plate boundary fault at ~820 mbsf that ruptured during the 2011 Mw 9.0 Tohoku earthquake but no clear breakouts were identified below the plate boundary fault (Lin et al., 2013). It is suggested that breakout-like structures and/or washouts occurred, which also form by compressive failure, but their occurrence and width were inconsistent not allowing stress analysis (Fig. S10). To compare the ASR stress orientations and the breakout data, we plotted the maximum horizontal stress (S_{Hmax}) azimuths of ASR1, 2 and 4 on the azimuth depth profile from breakout analysis by Lin et al. (2013) in Fig. 8(a).

The S_{Hmax} azimuth by breakout data looks to have a systematic change above ~140 mbsf, but the S_{Hmax} azimuth is highly variable from ~140 to ~450 mbsf, i.e., in the bottom part of Log unit I (slope sediments) and upper part of Log unit II (Log unit IIa). The ASR measurement at ~177 mbsf (ASR-1) reveals an S_{Hmax} azimuth approximately parallel to the plate motion direction (Fig. 8). More importantly, its intermediate principal strain (ε_2) and the minimum strain (ε_3) in the horizontal plane are almost the same, resulting in the same S_{Hmax} and S_{hmin} at a resolution of 0.1 MPa (Fig. 5(a) and Table 2). Although only one core sample was obtained and used for ASR measurement, these ASR data support the interpretation that S_{Hmax} and S_{hmin} are close in magnitude, therefore localized stress perturbations can be responsible for the scattered distribution of the S_{Hmax} azimuth suggested by Lin et al. (2013).

At a depth of ~697 mbsf of ASR-2 in Log unit IIb, the azimuth of S_{Hmax} as one of the two-dimensional principal stresses by ASR measurements is completely consistent with the breakout analyses. In addition, the three-dimensional principal stresses σ_1 and σ_2 plunge within 39–49° from the horizontal plane. This result likely reflects the stress state at depths of ~120 m above the plate boundary fault in the wedge sediments in the frontal accretionary prism. Although the small test number (only one) may have some uncertainty, the availability to determine the inclined σ_1 axis is an advantage of the three-dimensional ASR method over two-dimensional methods.

At a depth of ~828 mbsf of ASR-4, which is slightly below the plate boundary fault, the S_{Hmax} azimuth from the ASR measurements is nearly consistent with that of the breakout analyses above the fault (Fig. 8(a)). This depth of ASR-4 was defined as in Log unit III by geophysical log data and in Lithologic unit 5 (brown mudstone) by the lithology of core samples and was interpreted as underthrust sediments, i.e., representing the underthrust incoming plate (Expedition 343/343T Scientist, 2013b). To date, no directly measured result has been obtained by JFAST drilling or other studies that reveal the stress state below the plate boundary fault in the Japan trench both before and after the 2011 Mw 9.0 Tohoku earthquake. Therefore, this new data in the upper part of the incoming Pacific plate showing a normal faulting stress regime with a nearly parallel S_{Hmax} orientation with the plate convergence direction may be valuable in deepening our understanding of the mechanisms of great subduction zone seismogenesis and to simulate coseismic fault rupturing and propagating behavior and tsunamigenesis in the Japan trench.

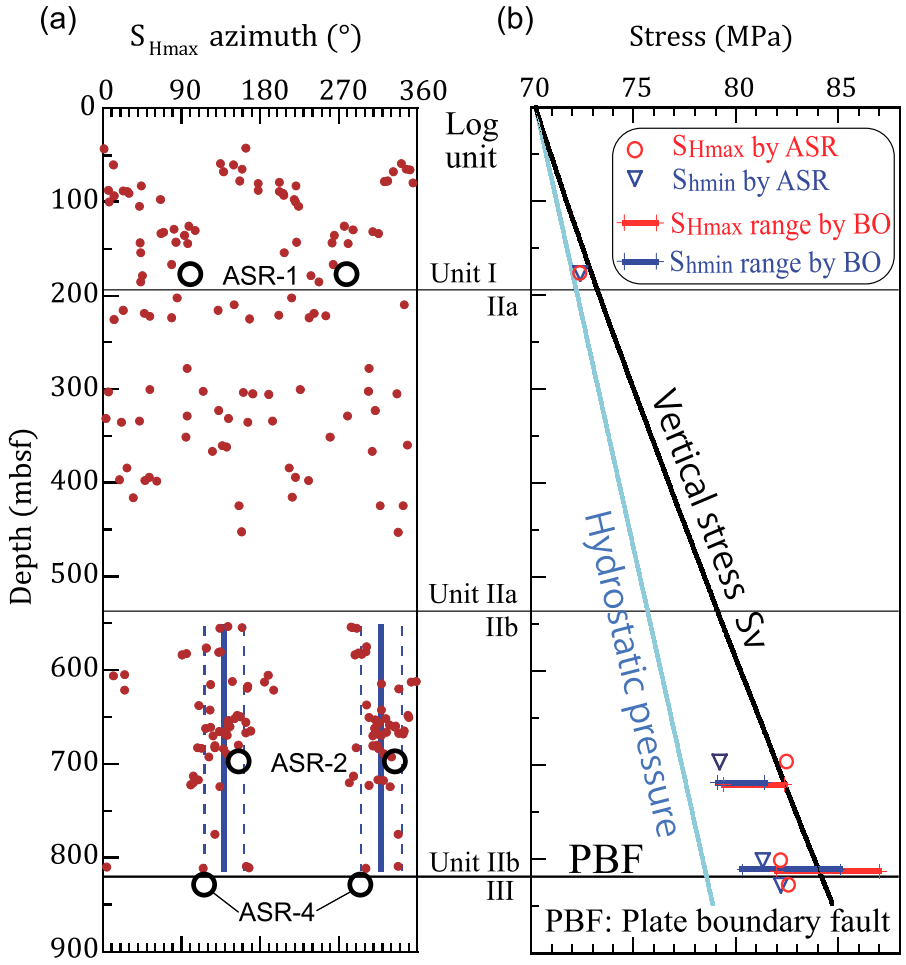

Fig. 8. Comparison between (a) S_{Hmax} azimuths determined from ASR (black open circles) and breakouts (red dots) and (b) S_{Hmax} and S_{hmin} magnitudes of ASR data (red circles and blue triangles) and breakout data (red and blue bars). Blue solid and dashed vertical lines in (a) show the mean and SD of S_{Hmax} azimuth (mean ± SD: 139 ± 23° or 319 ± 23°) in the Log unit IIb above the plate boundary fault obtained by breakout analyses (Lin et al., 2013). Stress magnitude S_V (black) in (b) was calculated from the rock formation density distribution shown in Fig. S8; hydrostatic pressure was calculated based on a sea water density 1.040 g/cm^3. S_{Hmax} and S_{hmin} ranges were constrained from breakout (BO) widths and rock compressive strengths by Lin et al. (2013).

4.2. Comparisons of stress magnitudes with previous breakout data

In addition to Table 2 providing the magnitudes of three-dimensional principal stresses and Fig. 7 showing the plots of two-dimensional horizontal principal stresses in stress polygon domains, we drew a depth profile of the horizontal principal stresses estimated from ASR measurements for comparison with the previous breakout data (Fig. 8(b)).

At a shallow depth of ~177 mbsf in the slope sediments, the ASR data show a "stress state at rest" in which the vertical stress S_v is almost the same as the maximum principal stress σ_1, and σ_2 (equal to S_{Hmax}) and σ_3 (S_{hmin}) are the same (Table 2, Figs. 7 and 8(b)). This stress state is an state caused by gravitation only but without the effects of tectonic loading of plate subduction. We are considering that the result is probably caused by two mechanisms. First, the ~50 m coseismic displacement during the 2011 Mw 9.0 earthquake resulted in a complete release of the tectonic horizontal stresses. Similarly, a model of shallow viscoelastic relaxation caused by coseismic stress release was proposed to explain tension cracks induced by megathrust earthquakes observed in Chile-Peru forearc (Luo et al., 2019). The second possibility is that the weak slope sediment formation with a high porosity of ~67% and probably a lower elastic Young's modulus does not accumulate tectonic stress accompanying plate subduction. We prefer to interpret the first one as the dominant reason, probably with some effects of the second.

Around the depth of ASR-3 in the wedge sediments close to (~18 m above) the plate boundary fault ruptured during the 2011 Tohoku earthquake, S_{Hmax} and S_{hmin} show a similar stress magnitude, having only a small differential stress (S_{Hmax} - S_{hmin}) of ≤1 MPa by the ASR method for different compliance ratios (Table 2 and Fig. 8(b)). The ASR stress magnitudes are within the stress range estimated by Lin et al. (2013) and are more consistent with those proposed by Brodsky et al. (2017). Brodsky et al. (2017) reanalyzed the same breakout data as Lin et al. (2013) by incorporating new and more robust laboratory constraints on rock strength and then determined a narrower stress magnitude distribution than that of Lin et al. (2013).

At a depth of ~828 mbsf in the underthrust sediments (~8 m below the plate boundary fault), the ASR stress magnitudes of S_{Hmax} and S_{hmin} show very similar values, and the differential stress between them (S_{Hmax} - S_{hmin}) is ≤0.5 MPa (Table 2 and Fig. 8(b)). We interpret that such small differential stress after the earthquake indicates that the tectonic stresses accumulated prior to the thrust earthquake were completely released coseismically. This interpretation is consistent with previous studies (Hasegawa et al., 2011; Lin et al., 2013; Brodsky et al., 2017). In addition, this stress state is very close to that of ASR-3 above the fault although orientation for ASR-3 is unknown. Therefore, the results of ASR-3 and ASR-4, including both the normal faulting stress regime and the horizontal principal stress magnitudes, suggest that the postearthquake stress states across the plate boundary fault rup-

tured during the 2011 Mw 9.0 earthquake are almost the same. However, it can be considered that the stress state in the oceanic crust (basalt) could differ from that in the narrow underthrust sediments indicated as the result of ASR-4.

5. Conclusions

The JFAST borehole penetrated the plate boundary fault between the subducting Pacific plate and overriding North American plate ruptured during the 2011 Mw 9.0 Tohoku earthquake in the area with the largest fault slip displacement close to the Japan trench. To supplement the lack of stress data below the rupture zone of the earthquake, we conducted core-based stress measurements by the anelastic strain recovery (ASR) method using four whole-round core samples of sediments retrieved from depths of ~177, ~687, ~802 and ~828 below sea floor (mbsf) called ASR-1 to −4, respectively, in borehole C0019E. In particular, stress data at ~828 mbsf can be analyzed for the first time from the foot wall of the fault. Consequently, the conclusions obtained in this study are helpful in enhancing our understanding of the mechanisms of great subduction zone earthquake occurrence and to simulate coseismic fault rupturing behavior.

(1) The postearthquake three-dimensional stress magnitudes at ~802 and ~828 mbsf across the plate boundary fault reveal a normal faulting stress regime in both the hanging wall and footwall of the plate boundary fault. The differences between the three-dimensional intermediate principal stress σ_2 and the minimum principal stress σ_3 at the two depths are less than 1 MPa, suggesting a complete release of horizontal tectonic stresses accumulated before the earthquake. In addition, the two-dimensional stress magnitudes of the maximum horizontal stress S_{Hmax} and the minimum horizontal stress S_{hmin} at the two depths also show similar results as the three-dimensional data.

(2) The S_{Hmax} azimuth N115°E at ~828 mbsf below the plate boundary fault from ASR measurements is consistent with the S_{Hmax} azimuth N139 ± 23°E (mean ± standard deviation) at ~550–810 mbsf belonging to Log unit IIb immediately above the fault. Taken together with the similar stress magnitudes at ~802 and ~828 mbsf, we interpret that the postearthquake stress states are almost the same in the sediments above and below the plate boundary fault. In other words, the stress state in terms of both orientation and magnitude is continuous across the fault.

(3) At a depth of ~177 mbsf in the slope sediments, the ASR stress data reveal a "stress state at rest", which is free from the tectonic effects of plate subduction. This fact could likely be attributed to the reset of the stress state by the great coseismic displacement of ~50 m slipped during the Tohoku earthquake.

CRediT authorship contribution statement

WL proposed the topic, conceived and designed the study. WL and TH carried out the ASR measurements onboard D/V *Chikyu*; YY carried out the core reorientation experiments. WL wrote the draft and created the figures. All authors reviewed and improved the manuscript, also read through and approved the final manuscript.

Declaration of competing interest

The authors declare that they have no known competing financial interests or personal relationships that could have appeared to influence the work reported in this paper.

Data availability

We have submitted the data as supplemental materials with this paper.

Acknowledgements

The core samples used in this study were provided by IODP Expedition 343. The authors gratefully acknowledge the support provided by the Expedition 343/343T co-chief scientists Jim Mori and Fred Chester, EPMs, the other Expedition scientists, laboratory technicians, and D/V *Chikyu* drilling crew. The authors also thank Osamu Tadai for his helps to sub-sample preparations for core reorientation experiments in Kochi Core Center, Japan. The authors sincerely thank two reviewers (Tim Byrne and an anonymous reviewer) for their careful reviewing and valuable comments which helped us to improve our manuscript. This work was partially supported by JSPS KAKENHI Grant Number JP25287134 and JP19H00717.

Appendix A. Supplementary material

Supplementary material related to this article can be found online at https://doi.org/10.1016/j.epsl.2022.117888.

References

Argus, D.F., Gordon, R.G., DeMets, C., 2011. Geologically current motion of 56 plates relative to the no-net-rotation reference frame. Geochem. Geophys. Geosyst. 12, Q11001. https://doi.org/10.1029/2011GC003751.

Brodsky, E.E., Saffer, D., Fulton, P., Chester, F., Conin, M., Huffman, K., Moore, J.C., Wu, H.-Y., 2017. The postearthquake stress state on the Tohoku megathrust as constrained by reanalysis of the JFAST breakout data. Geophys. Res. Lett. 44, 8294–8302. https://doi.org/10.1002/2017GL074027.

Brodsky, E., Mori, J., Anderson, L., Behrmann, J., Bose, S., Chester, F., Conin, M., Cook, B., Eguchi, N., Fulton, P., Hino, R., Hirose, T., Ikari, M., Ishikmawa, T., Jeppson, T., Kano, Y., Kirkpatrick, J., Kodaira, S., Lin, W., Maeda, L., Mishima, T., Moore, C., Nakamura, Y., Rabinowicz, H., Regalla, C., Remitti, F., Rowe, C., Saffer, D., Saito, S., Sample, J., et al., 2020. The state of stress on the fault before, during, and after a major earthquake. Annu. Rev. Earth Planet. Sci. 48, 49–74. https://doi.org/10.1146/annurev-earth-053018-060507.

Byrne, T., Lin, W., Tsutsumi, A., Yamamoto, Y., Lewis, J., Kanagawa, K., Kitamura, Y., Yamaguchi, A., Kimura, G., 2009. Anelastic strain recovery reveals extension across SW Japan subduction zone. Geophys. Res. Lett. 36, L01305. https://doi.org/10.1029/2009GL040749.

Chester, F.M., Mori, J.J., Toczko, S., Eguchi, N., Expedition 343/343T Scientists, 2012. Japan trench fast drilling project (JFAST). IODP Prel. Rep. 343/343T. https://doi.org/10.2204/iodp.pr.343343T.2012.

Chester, F.M., Rowe, C., Ujiie, K., Kirkpatrick, J., Regalla, C., Remitti, F., Moore, J.C., Toy, V., Wolfson-Schwehr, M., Bose, S., Kameda, J., Mori, J.J., Brodsky, E.E., Eguchi, N., Toczko, S., Expedition 343 and 343T Scientists, 2013. Structure and composition of the plate-boundary slip zone for the 2011 Tohoku-Oki earthquake. Science 342, 1208–1211. https://doi.org/10.1126/science.1243719.

Cui, J., Lin, W., Wang, L., Gao, L., Huang, Y., Wang, W., Sun, D., Li, Z., Zhou, J., Qian, H., Peng, H., Xia, K., Li, K., 2014. Determination of three-dimensional in situ stresses by anelastic strain recovery in Wenchuan Earthquake Fault Scientific Drilling Project Hole-1 (WFSD-1). Tectonophysics 619–620, 123–132. https://doi.org/10.1016/j.tecto.2013.09.013.

Expedition 343/343T Scientists, 2013a. Expedition 343/343T summary. In: Chester, F.M., Mori, J., Eguchi, N., Toczko, S., Expedition 343/343T Scientists (Eds.), Proceedings of the IODP, vol. 343/343T. Integrated Ocean Drilling Program Management International, Inc., Tokyo.

Expedition 343/343T Scientists, 2013b. Site C0019. In: Chester, F.M., Mori, J., Eguchi, N., Toczko, S., Expedition 343/343T Scientists (Eds.), Proceedings of the IODP, vol. 343/343T. Integrated Ocean Drilling Program Management International, Inc., Tokyo.

Fujiwara, T., Kodaira, S., No, T., Kaiho, Y., Takahashi, N., Kaneda, Y., 2011. The 2011 Tohoku-Oki earthquake: displacement reaching the trench axis. Science 334, 1240. https://doi.org/10.1126/science.1211554.

Fulton, P.M., Brodsky, E.E., Kano, Y., Mori, J., Chester, F., Ishikawa, T., Harris, R.N., Lin, W., Eguchi, N., Toczko, S., Expedition 343, 343T, and KR13-08 Scientists, 2013. Low coseismic friction on the Tohoku-Oki fault determined from temperature measurements. Science 342, 1214–1217. https://doi.org/10.1126/science.1243641.

Gao, L., Lin, W., Sun, D., Wang, H., 2014. Experimental anelastic strain recovery compliance of three typical rocks. Rock Mech. Rock Eng. 47, 1987–1995. https://doi.org/10.1007/s00603-013-0526-0.

Hasegawa, A., Yoshida, K., Okada, T., 2011. Nearly complete stress drop in the 2011 Mw 9.0 off the Pacific coast of Tohoku earthquake. Earth Planets Space 63, 703. https://doi.org/10.5047/eps.2011.06.007.2011.

Hasegawa, A., Yoshida, K., Asano, Y., Okada, T., Iinuma, T., Ito, Y., 2012. Change in stress field after the 2011 great Tohoku–Oki earthquake. Earth Planet. Sci. Lett. 355–356, 231–243. https://doi.org/10.1016/j.epsl.2012.08.042.

Iinuma, T., Hino, R., Kido, M., Inazu, D., Osada, Y., Ito, Y., Ohzono, M., Tsushima, H., Suzuki, S., Fujimoto, H., Miura, S., 2012. Coseismic slip distribution of the 2011 off the Pacific coast of Tohoku earthquake (M9.0) refined by means of seafloor geodetic data. J. Geophys. Res. 117, B07409. https://doi.org/10.1029/2012JB009186.

Kanamori, H., Brodsky, E.E., 2001. The physics of earthquakes. Phys. Today 54, 34–40. https://doi.org/10.1063/1.1387590.

Kodaira, S., No, T., Nakamura, Y., Fujiwara, T., Kaiho, Y., Miura, S., Takahashi, N., Kaneda, Y., Taira, A., 2012. Coseismic fault rupture at the trench axis during the 2011 Tohoku-oki earthquake. Nat. Geosci. 5, 646–650. https://doi.org/10.1038/NGEO1547.

Lay, T., Ammon, C.J., Kanamori, H., Xue, L., Kim, M.J., 2011. Possible large near-trench slip during the 2011 Mw 9.0 off the Pacific coast of Tohoku earthquake. Earth Planets Space 63, 687–692. https://doi.org/10.5047/eps.2011.05.033.

Lin, W., Kwasniewski, M., Imamura, T., Matsuki, K., 2006. Determination of three-dimensional in-situ stresses from anelastic strain recovery measurement of cores at great depth. Tectonophysics 426, 221–238. https://doi.org/10.1016/j.tecto.2006.02.019.

Lin, W., Yeh, E., Ito, H., Hirono, T., Soh, W., Wang, C.-Y., Ma, K.-F., Hung, J.-H., Song, S.-R., 2007. Preliminary results of stress measurement using drill cores of TCDP Hole-A: an application of anelastic strain recovery method to three dimensional in situ stress determination. Terr. Atmos. Ocean. Sci. 18, 379–393. https://doi.org/10.3319/TAO.2007.18.2.379(TCDP).

Lin, W., Saito, S., Sanada, Y., Yamamoto, Y., Hashimoto, Y., Kanamatsu, T., 2011. Principal horizontal stress orientations prior to the 2011 M_w 9.0 Tohoku-Oki, Japan, earthquake in its source area. Geophys. Res. Lett. 38, L00G10. https://doi.org/10.1029/2011GL049097.

Lin, W., Conin, M., Moore, J.C., Chester, F.M., Nakamura, Y., Mori, J.J., Anderson, L., Brodsky, E.E., Eguchi, H., Expedition 343 Scientists, 2013. Stress state in the largest displacement area of the 2011 Tohoku-Oki earthquake. Science 339, 687–690. https://doi.org/10.1126/science.1229379.

Lin, W., Fulton, P.M., Harris, R.N., Tadai, O., Matsubayashi, O., Tanikawa, W., Kinoshita, M., 2014. Thermal conductivities, thermal diffusivities, and volumetric heat capacities of core samples obtained from the Japan Trench Fast Drilling Project (JFAST). Earth Planets Space 66, 48. https://doi.org/10.1186/1880-5981-66-48.

Loveless, J.P., Meade, B.J., 2010. Geodetic imaging of plate motions, slip rates, and partitioning of deformation in Japan. J. Geophys. Res. 115, B02410. https://doi.org/10.1029/2008JB006248.

Luo, H., Wang, K., Sone, H., He, J., 2019. A model of shallow viscoelastic relaxation for seismically induced tension cracks in the Chile-Peru forearc. Geophys. Res. Lett. 46, 10,773–10,781. https://doi.org/10.1029/2019GL084536.

Matsuki, K., 1991. Three-dimensional in situ stress measurement with anelastic strain recovery of a rock core. In: Wittke, W. (Ed.), Book Proc. 7th Int. Congr. Rock Mech., Aachen, vol. 1, pp. 557–560.

Matsuki, K., Takeuchi, K., 1993. Three-dimensional in situ stress determination by anelastic strain recovery of a rock core. Int. J. Rock Mech. Min. Sci. Geomech. Abstr. 30, 1019–1022.

Matsuki, K., 2008. Anelastic strain recovery compliance of rocks and its application to in situ stress measurement. Int. J. Rock Mech. Min. Sci. Geomech. Abstr. 45, 952–965. https://doi.org/10.1016/j.ijrmms.2007.10.005.

Mori, J.J., Chester, F.M., Eguchi, N., Toczko, S., 2012. Japan Trench Fast Earthquake Drilling Project (JFAST). IODP Sci. Prosp. 343. https://doi.org/10.2204/iodp.sp.343.2012.

Mori, J., Chester, F., Brodsky, E., Kodaira, S., 2014. Investigation of the huge tsunami from the 2011 Tōhoku-Oki, Japan, earthquake using ocean floor boreholes to the fault zone. Oceanography 27, 132–137. https://doi.org/10.5670/oceanog.2014.48.

Nagano, Y., Lin, W., Yamamoto, K., 2015. In-situ stress analysis using the anelastic strain recovery (ASR) method at the first offshore gas production test site in the eastern Nankai Trough, Japan. Mar. Pet. Geol. 66, 418–424. https://doi.org/10.1016/j.marpetgeo.2015.02.027.

Oohashi, K., Lin, W., Wu, H., Yamaguchi, A., Yamamoto, Y., 2017. Stress state in the Kumano basin and in slope sediment determined from anelastic strain recovery: results from IODP expedition 338 to the Nankai Trough. Geochem. Geophys. Geosyst. 18, 3608–3616. https://doi.org/10.1002/2017GC007137.

Rowe, C.D., Moore, J.C., Remitti, F., the IODP Expedition 343/343T Scientists, 2013. The thickness of subduction plate boundary faults from the seafloor into the seismogenic zone. Geology 41, 991–994. https://doi.org/10.1130/G34556.1.

Sugimoto, T., Yamamoto, Yuhji, Yamamoto, Yuzuru, Lin, W., 2020. A method for core reorientation based on rock remanent magnetization: application to hemipelagic sedimentary soft rock. Mater. Trans. 61, 1638–1644. https://doi.org/10.2320/matertrans.Z-M2020832.

Sun, D., Sone, H., Lin, W., Cui, J., He, B., Lv, H., Cao, Z., 2017. Stress state measured at ~7 km depth in the Tarim Basin, NW China. Sci. Rep. 7, 4503. https://doi.org/10.1038/s41598-017-04516-9.

Terakawa, T., Matsu'ura, M., 2010. The 3-D tectonic stress fields in and around Japan inverted from centroid moment tensor data of seismic events. Tectonics 29, TC6008. https://doi.org/10.1029/2009TC002626.

Townend, J., Zoback, M.D., 2006. Stress, strain, and mountain building in central Japan. J. Geophys. Res. 111, B03411. https://doi.org/10.1029/2005JB003759.

Wang, K., Suyehiro, K., 1999. How does plate coupling affect crustal stresses in Northeast and Southwest Japan? Geophys. Res. Lett. 26, 2307–2310. https://doi.org/10.1029/1999GL900528.

Ujiie, K., Tanaka, H., Saito, T., Tsutsumi, A., Mori, J.J., Kameda, J., Brodsky, E.E., Chester, F.M., Eguchi, N., Toczko, S., Expedition 343 and 343T Scientists, 2013. Low coseismic shear stress on the Tohoku-Oki Megathrust determined from laboratory experiments. Science 342, 1211–1214. https://doi.org/10.1126/science.1243485.

Yamamoto, Yuzuru, Lin, W., Oda, H., Byrne, T., Yamamoto, Yuhji, 2013. Stress states at the subduction input site, Nankai Subduction Zone, using anelastic strain recovery (ASR) data in the basement basalt and overlying sediments. Tectonophysics 600, 91–98. https://doi.org/10.1016/j.tecto.2013.01.028.

Yamanaka, Y., Kikuchi, M., 2004. Asperity map along the subduction zone in northeastern Japan inferred from regional seismic data. J. Geophys. Res. 109, B07307. https://doi.org/10.1029/2003JB002683.

Yang, T., Mishima, T., Ujiie, K., Chester, F.M., Mori, J.J., Eguchi, N., Toczko, S., Expedition 343 Scientists, 2013. Strain decoupling across the décollement in the region of large slip during the 2011 Tohoku-Oki earthquake from anisotropy of magnetic susceptibility. Earth Planet. Sci. Lett. 381 (C), 31–38. https://doi.org/10.1016/j.epsl.2013.08.045.

Yoshida, K., Hasegawa, A., Okada, T., Iinuma, T., Ito, Y., Asano, Y., 2012. Stress before and after the 2011 Great Tohoku-oki earthquake and induced earthquakes in inland areas of eastern, Japan. Geophys. Res. Lett. 39, L03302. https://doi.org/10.1029/2011GL049729.

Yoshida, K., Hasegawa, A., Okada, T., 2015. Spatial variation of stress orientations in NE Japan revealed by dense seismic observations. Tectonophysics 647–648, 63–72. https://doi.org/10.1016/j.tecto.2015.02.013.

Zhang, C., Lin, W., He, M., Tao, Z., Meng, W., 2022. Determining in-situ stress state by anelastic strain recovery method beneath Xiamen: implications for the coastal region of Southeastern China. Rock Mech. Rock Eng. 55, 5687–5703. https://doi.org/10.1007/s00603-022-02915-7.

Zoback, M.D., 2007. Reservoir Geomechanics. Cambridge Univ. Press, Cambridge.